

Signatures of a Light Sterile Neutrino in T2HK

Sanjib Kumar Agarwalla,^{a,b,c} **Sabya Sachi Chatterjee**,^{a,b} **Antonio Palazzo**^{d,e}

^a*Institute of Physics, Sachivalaya Marg, Sainik School Post, Bhubaneswar 751005, India*

^b*Homi Bhabha National Institute, Training School Complex, Anushakti Nagar, Mumbai 400085, India*

^c*International Centre for Theoretical Physics, Strada Costiera 11, Trieste 34151, Italy*

^d*Dipartimento Interateneo di Fisica “Michelangelo Merlin”, Via Amendola 173, 70126 Bari, Italy*

^e*Istituto Nazionale di Fisica Nucleare (INFN), Sezione di Bari, Via E. Orabona 4, I-70126 Bari, Italy*

E-mail: sanjib@iopb.res.in, sabya@iopb.res.in, palazzo@ba.infn.it

ABSTRACT: We investigate the performance of T2HK in the presence of a light eV scale sterile neutrino. We study in detail its influence in resolving fundamental issues like mass hierarchy, CP-violation (CPV) induced by the standard CP-phase δ_{13} and new CP-phase δ_{14} , and the octant ambiguity of θ_{23} . We show for the first time in detail that due to the impressive energy reconstruction capabilities of T2HK, the available spectral information plays an important role to enhance the mass hierarchy discovery reach of this experiment in 3ν framework and also to keep it almost intact even in 4ν scheme. This feature is also of the utmost importance in establishing the CPV due to δ_{14} . As far as the sensitivity to CPV due to δ_{13} is concerned, it does not change much going from 3ν to 4ν case. We also examine the reconstruction capability of the two phases δ_{13} and δ_{14} , and find that the typical 1σ uncertainty on δ_{13} (δ_{14}) in T2HK is $\sim 15^0$ (30^0). While determining the octant of θ_{23} , we face a complete loss of sensitivity for unfavorable combinations of unknown δ_{13} and δ_{14} .

KEYWORDS: Neutrino Oscillation, Long-baseline, Sterile Neutrino, T2HK

ARXIV EPRINT: [1801.aaaaaa](https://arxiv.org/abs/1801.04855)

Contents

| | | |
|----------|--|-----------|
| 1 | Introduction and Motivation | 1 |
| 2 | Transition probability in the 3+1 scheme | 2 |
| 2.1 | Theoretical framework | 2 |
| 2.2 | Transition probability | 3 |
| 3 | Details of the numerical analysis | 3 |
| 3.1 | T2HK setup | 3 |
| 3.2 | Statistical Method | 4 |
| 4 | Mass hierarchy discovery potential in the 3+1 scheme | 7 |
| 5 | CP-violation searches in the 3+1 scheme | 9 |
| 5.1 | CP-violation discovery potential | 9 |
| 5.2 | Reconstruction of the CP phases | 14 |
| 6 | Sensitivity to the octant of θ_{23} | 16 |
| 7 | Conclusions and Outlook | 17 |

1 Introduction and Motivation

Sterile neutrinos, neutral singlets of the $SU(2)_L$ weak isospin group, are perhaps the simplest extension of the Standard Model. Intriguingly, a series of anomalies detected at the short baseline (SBL) experiments, support the existence of one or more sterile states (see [1–3] for a review of the topic) at the scale of ~ 1 eV.

New SBL experiments will be able to test such a hypothesis (see the review in [4]) seeking the typical L/E pattern induced by the oscillations driven by the new mass-squared splitting(s) $\Delta m_{new}^2 \sim 1$ eV². However, after a hypothetical discovery, the complete mapping of the parameters regulating the oscillation process would require other kinds of experiments. In fact, even in the simplest scenario, the so called 3+1 scheme, where only one sterile state participates to the oscillations, there are three new mixing angles and two new CP violating phases in addition to the standard 3-flavor parameters.

The CP phases (both standard and non-standard) can be observed solely through interference effects between two distinct oscillation frequencies. In the 3+1 scheme, at SBL setups, only one frequency is observable (the new one) while the atmospheric and solar frequencies are basically invisible. This drastically suppresses the amplitude of any interference effect, and, as a consequence, the SBL experiments are completely blind to the CP violation phases.

As first shown in [5], the situation is qualitatively different at the long baseline (LBL) experiments, because in these setups the interference between two distinct frequencies shows up. In this way the LBL experiments acquire sensitivity both to the standard CP phase and to the new ones. Therefore, the LBL setups have a complementary role to the SBL experiments in the searches for the sterile neutrino properties.

The next-generation LBL neutrino oscillation experiments [6–10], would naturally play a crucial role in this arena. In the present work, we focus on the proposed experiment Tokai to Hyper Kamiokande (T2HK), which will make use of a very powerful neutrino beam shot from Tokai to Kamioka over a distance of 295 km. Our work complements other recent studies performed about DUNE [11–14] and T2HK [15, 16]. Previous studies on sterile neutrinos at LBL experiments can be found in [17–25].

The paper is organized as follows. In section 2, we present the theoretical framework and discuss the behavior of the 4-flavor $\nu_\mu \rightarrow \nu_e$ conversion probability. In section 3, we describe the details of the T2HK setup and of the numerical analysis. In section 4, we present the sensitivity study of the mass hierarchy. Section 5 deals with the CPV discovery potential and the reconstruction capability of the CP phases. Section 6 is devoted to the assessment of the capability of reconstructing the octant of θ_{23} . Finally, we draw our conclusions in section 7.

2 Transition probability in the 3+1 scheme

2.1 Theoretical framework

In the 3+1 scheme, the four flavor eigenstates $(\nu_e, \nu_\mu, \nu_\tau, \nu_s)$ are related to the mass eigenstates $(\nu_1, \nu_2, \nu_3, \nu_4)$ through a 4×4 unitary matrix, which can be written in the following fashion

$$U = \tilde{R}_{34} R_{24} \tilde{R}_{14} R_{23} \tilde{R}_{13} R_{12}, \quad (2.1)$$

where R_{ij} (\tilde{R}_{ij}) is a real (complex) 4×4 rotation matrix with a mixing angle θ_{ij} and containing the 2×2 submatrix

$$R_{ij}^{2 \times 2} = \begin{pmatrix} c_{ij} & s_{ij} \\ -s_{ij} & c_{ij} \end{pmatrix}, \quad \tilde{R}_{ij}^{2 \times 2} = \begin{pmatrix} c_{ij} & \tilde{s}_{ij} \\ -\tilde{s}_{ij}^* & c_{ij} \end{pmatrix}, \quad (2.2)$$

in the (i, j) sub-block with

$$c_{ij} \equiv \cos \theta_{ij}, \quad s_{ij} \equiv \sin \theta_{ij}, \quad \tilde{s}_{ij} \equiv s_{ij} e^{-i\delta_{ij}}. \quad (2.3)$$

The parameterization adopted in Eq. (2.1) has several merits: i) In the limiting case in which there is no mixing of the active states with the sterile one ($\theta_{14} = \theta_{24} = \theta_{34} = 0$), it gives back the 3-flavor matrix in its usual parameterization. ii) For small values of θ_{13} , θ_{14} , and θ_{24} , one has $|U_{e3}|^2 \simeq s_{13}^2$, $|U_{e4}|^2 = s_{14}^2$, $|U_{\mu 4}|^2 \simeq s_{24}^2$, and $|U_{\tau 4}|^2 \simeq s_{34}^2$, with a transparent physical interpretation of the new mixing angles. iii) The leftmost positioning of the rotation matrix \tilde{R}_{34} makes the vacuum $\nu_\mu \rightarrow \nu_e$ transition probability independent of θ_{34} and of the associated CP phase δ_{34} (see [5]).

2.2 Transition probability

For the T2HK baseline (295 km), matter effects are not significant. Therefore, we can restrict our analytical discussion to the vacuum case. As discussed in [5], the $\nu_\mu \rightarrow \nu_e$ transition probability can be expressed as the sum of three terms

$$P_{\mu e}^{4\nu} \simeq P_{\mu e}^{\text{ATM}} + P_{\mu e}^{\text{INT I}} + P_{\mu e}^{\text{INT II}}. \quad (2.4)$$

The first term is controlled by the atmospheric mass-squared splitting and acts as the leading contributor to the conversion probability. We can write this positive-definite term in the following way

$$P_{\mu e}^{\text{ATM}} \simeq 4s_{23}^2 s_{13}^2 \sin^2 \Delta, \quad (2.5)$$

where $\Delta \equiv \Delta m_{31}^2 L / 4E$ is the atmospheric oscillating factor, where E is the neutrino energy and L is the baseline. The second and third terms in Eq. (2.4) are due to interference and can assume both positive and negative values. The second term is related to the solar-atmospheric interference and can be written as

$$P_{\mu e}^{\text{INT I}} \simeq 8s_{13}s_{12}c_{12}s_{23}c_{23}(\alpha\Delta) \sin \Delta \cos(\Delta + \delta_{13}). \quad (2.6)$$

The third term comes into the picture as a genuine 4-flavor effect, and is related to the atmospheric-sterile interference. It has the following form [5]

$$P_{\mu e}^{\text{INT II}} \simeq 4s_{14}s_{24}s_{13}s_{23} \sin \Delta \sin(\Delta + \delta_{13} - \delta_{14}). \quad (2.7)$$

From the previous three expressions, we see that the conversion probability depends on three small mixing angles: θ_{13} , θ_{14} , and θ_{24} . Interesting to note that the best estimates of these three mixing angles (determined in the 3-flavor framework [26–28] for θ_{13} , and in the 3+1 scheme [29–31] for θ_{14} and θ_{24}) are quite similar and we have $s_{13} \sim s_{14} \sim s_{24} \sim 0.15$ (see table 1). Therefore, it makes perfect sense to treat these three mixing angles θ_{13} , θ_{14} , and θ_{24} as small quantities having the same order ϵ . Conversely, the ratio of the solar over the atmospheric mass-squared splitting, $\alpha \equiv \Delta m_{21}^2 / \Delta m_{31}^2 \simeq \pm 0.03$ turns out to be of order ϵ^2 . From Eqs. (2.5)–(2.7), we see that the first (leading) term is of the second order in ϵ , while both the second and third (subleading) interference terms are of the third order in ϵ . Hence, the sizes of the two interference terms are expected to be similar.

3 Details of the numerical analysis

3.1 T2HK setup

The main objective of the long-baseline neutrino program at the proposed Hyper-Kamiokande (HK) detector with an intense neutrino beam from the J-PARC proton synchrotron is to provide a conclusive evidence for leptonic CP-violation in neutrino oscillations induced by an irreducible phase δ_{13} in the three-flavor neutrino mixing matrix. This setup is commonly known as “T2HK” (Tokai to Hyper-Kamiokande) experiment [32–34]. To estimate

the physics reach of this setup, we closely follow the experimental configurations as described in Ref. [33, 34]. The neutrino beam for HK will be produced at J-PARC from the collision of 30 GeV protons with a graphite target. In our simulation, we consider an integrated proton beam power of $7.5 \text{ MW} \times 10^7$ seconds, which can deliver in total 15.6×10^{21} protons on target (p.o.t.) with a 30 GeV proton beam. We assume that the T2HK experiment would use 25% of its full exposure in the neutrino mode which is 3.9×10^{21} p.o.t. and the remaining 75% (11.7×10^{21} p.o.t.) would be utilized during antineutrino run. In this way, we make sure that we have nearly equal statistics in both neutrino and antineutrino modes to optimize the search for leptonic CP-violation. These neutrinos and antineutrinos will be observed in the gigantic 560 kt (fiducial) HK water Cherenkov detector in the Tochibora mine, located 8 km south of Super-Kamiokande and 295 km away from J-PARC. The neutrino beamline from J-PARC is designed to accommodate an off-axis angle of $\sim 2.5^\circ$ at the proposed HK site and therefore, the beam peaks sharply at the first oscillation maximum of 0.6 GeV to enhance the physics sensitivity. This off-axis scheme [35] produces a neutrino beam with a narrow energy spectrum which substantially reduces the intrinsic ν_e contamination in the beam and also the background which stems from neutral current events. Therefore, the signal-to-background ratio gets improved significantly. In our analysis, we consider the reconstructed neutrino and antineutrino energy range of 0.1 GeV to 1.25 GeV for the appearance channel. In case of disappearance channel, the assumed energy range is 0.1 GeV to 7 GeV for both the ν_μ and $\bar{\nu}_\mu$ candidate events. We match all the signal and background event numbers following table 19 and 20 of ref. [33]. The systematic uncertainties play an important role in estimating the physics sensitivity of the T2HK setup. Following table 21 of ref. [33], we consider an uncorrelated normalization uncertainty of 3.5% for both appearance and disappearance channels in neutrino mode. In case of antineutrino run, the uncorrelated normalization uncertainties are 6% and 4.5% for appearance and disappearance channels respectively, and also, they do not have any correlation with appearance and disappearance channels in neutrino mode. We assume an uncorrelated 10% normalization uncertainty on background for both appearance and disappearance channels in neutrino and antineutrino modes. With all these assumptions on the T2HK setup, we manage to reproduce all the sensitivity results which are given in ref. [33]. Here, we would like to mention that according to the latest report by the Hyper-Kamiokande Proto-Collaboration [36], the total beam exposure is 27×10^{21} p.o.t. and the fiducial mass for the proposed HK detector is 374 kt. Comparing the exposures in terms of ($\text{kt} \times \text{p.o.t.}$), we see that our exposure is 1.156 times smaller than the exposure that has been considered in ref. [36]. But, certainly, the results presented in this work would not change much and the conclusions drawn based on these results would remain valid even if we consider the new exposure as reported in ref. [36].

3.2 Statistical Method

In this section, we briefly describe the numerical technique and analysis procedure that we adopt to produce our sensitivity results. To compute the experimental sensitivities, we rely on the well-known GLoBES software [37, 38] along with its new physics tools which estimates the median sensitivity of the experiment without including statistical fluctua-

| Parameter | True Value | Marginalization Range |
|---|--------------|-----------------------|
| $\sin^2 \theta_{12}$ | 0.304 | Not marginalized |
| $\sin^2 2\theta_{13}$ | 0.085 | Not marginalized |
| $\sin^2 \theta_{23}$ | 0.50 | [0.34, 0.68] |
| $\sin^2 \theta_{14}$ | 0.025 | Not marginalized |
| $\sin^2 \theta_{24}$ | 0.025 | Not marginalized |
| $\sin^2 \theta_{34}$ | 0.0 | Not marginalized |
| $\delta_{13}/^\circ$ | [- 180, 180] | [- 180, 180] |
| $\delta_{14}/^\circ$ | [- 180, 180] | [- 180, 180] |
| $\delta_{34}/^\circ$ | 0 | Not marginalized |
| $\frac{\Delta m_{21}^2}{10^{-5} \text{ eV}^2}$ | 7.50 | Not marginalized |
| $\frac{\Delta m_{31}^2}{10^{-3} \text{ eV}^2}$ (NH) | 2.475 | Not marginalized |
| $\frac{\Delta m_{31}^2}{10^{-3} \text{ eV}^2}$ (IH) | - 2.4 | Not marginalized |
| $\frac{\Delta m_{41}^2}{\text{eV}^2}$ | 1.0 | Not marginalized |

Table 1. Oscillation parameters considered in our analysis. The second column depicts the true values of the oscillation parameters used to simulate the “observed” data set. The third column shows the ranges over which $\sin^2 \theta_{23}$, δ_{13} , and δ_{14} are varied while minimizing the χ^2 to produce the final results.

tions. We make appropriate changes in the $\nu_\mu \rightarrow \nu_e$ and $\nu_\mu \rightarrow \nu_\mu$ transition probabilities to incorporate the 3+1 scheme with one light eV-scale sterile neutrino. We do the same for antineutrino as well. We observe that for the small values of mixing angles θ_{14} and θ_{24} considered in the present work (see table 1), the 4-flavor $\nu_\mu \rightarrow \nu_\mu$ disappearance probability is very similar to the 3ν case, which agrees with the findings in ref. [5]. In this paper, the strategy that we adopt for the statistical treatment, is exactly similar to what have been discussed in section 4 of ref. [39]. Table 1 depicts the true values of the oscillation parameters and their marginalization ranges which we consider in our simulation. Our benchmark

choices for the three-flavor neutrino oscillations parameters are in close agreement with the values obtained in the recent global fit studies [26–28]. As far as the atmospheric mixing angle is concerned, we consider maximal mixing¹ (45°) as the true choice, and in the fit, we marginalize over the range given in table 1. We present all the sensitivity results assuming normal hierarchy² (NH) as the true choice. For the CP-violation searches and the reconstruction of the CP phases, we show our results with and without marginalizing over both the choices of hierarchy in the fit, which enable us to see how much the sensitivities can be deteriorated due to the possible degeneracies between $\text{sgn}(\Delta m_{31}^2)$ and CP phases. While showing the results for the octant measurement of θ_{23} , we marginalize over both the choices of hierarchy in the fit. This issue of hierarchy marginalization in the fit becomes irrelevant in case of the mass hierarchy discovery studies where our aim is to exclude the wrong hierarchy in the fit. The true value of δ_{13} is varied in its allowed range of $[-\pi, \pi]$, and it has been marginalized over its full range in the fit if the analysis demands so. Following the Preliminary Reference Earth Model (PREM) [40], we take the line-averaged constant Earth matter density of 2.8 g/cm^3 for the T2HK baseline.

In our simulation, we consider the new mass-squared splitting Δm_{41}^2 to be 1 eV^2 as preferred by the recent short-baseline data. Here, we would like to mention that our sensitivity results would remain the same for other values of this parameter, provided that $\Delta m_{41}^2 \gtrsim 0.1 \text{ eV}^2$. The rapid oscillations induced by such large values of Δm_{41}^2 get completely averaged because of the finite resolution of the detector. Due to the same reason, the T2HK setup is insensitive to the sign of Δm_{41}^2 and we can safely assume it to be positive. As far as the active-sterile mixing angles are concerned, we take the true values of 0.025 for both $\sin^2 \theta_{14}$ and $\sin^2 \theta_{24}$ and keep them fixed in the fit. Our choices for these new mixing angles are quite close to the best-fit values obtained by the global 3+1 fits [29–31]. We vary the true value of δ_{14} in its allowed range of $[-\pi, \pi]$ and it has been marginalized over its full range in the fit as required. We consider $\theta_{34} = 0$ and $\delta_{34} = 0$ in our simulations³.

In our analysis, we do not explicitly simulate the near detector of T2HK which may provide some information regarding θ_{14} and θ_{24} , but surely, the near detector data is blind to the CP phases which we want to explore in this work. While producing our sensitivity results, we perform a full spectral analysis using the binned events spectra for the T2HK setup. Following refs. [41, 42], we use the well-known “pull” method to marginalize the Poissonian $\Delta\chi^2$ over the uncorrelated systematic uncertainties. We quote the statistical significance⁴ of our results for 1 d.o.f. in terms of $n\sigma$, where $n = \sqrt{\Delta\chi^2}$.

¹Latest 3ν global fits [26–28] prefer non-maximal θ_{23} with two nearly degenerate solutions: one $< 45^\circ$, known as lower octant (LO), and the other $> 45^\circ$, termed as higher octant (HO). But, maximal mixing is still allowed in 3σ range.

²We have checked that the results do not differ much if we generate the prospective data with inverted hierarchy (IH).

³In vacuum, $\nu_\mu \rightarrow \nu_e$ oscillation probability is independent of θ_{34} (and δ_{34}). For the T2HK baseline, the matter effect is very small and in the probability expression we see a very tiny dependence on these parameters which can be safely neglected. An analytical understanding of this issue is given in the appendix of ref. [5].

⁴For a detailed discussion on the statistical interpretation of oscillation experiments, see the recent

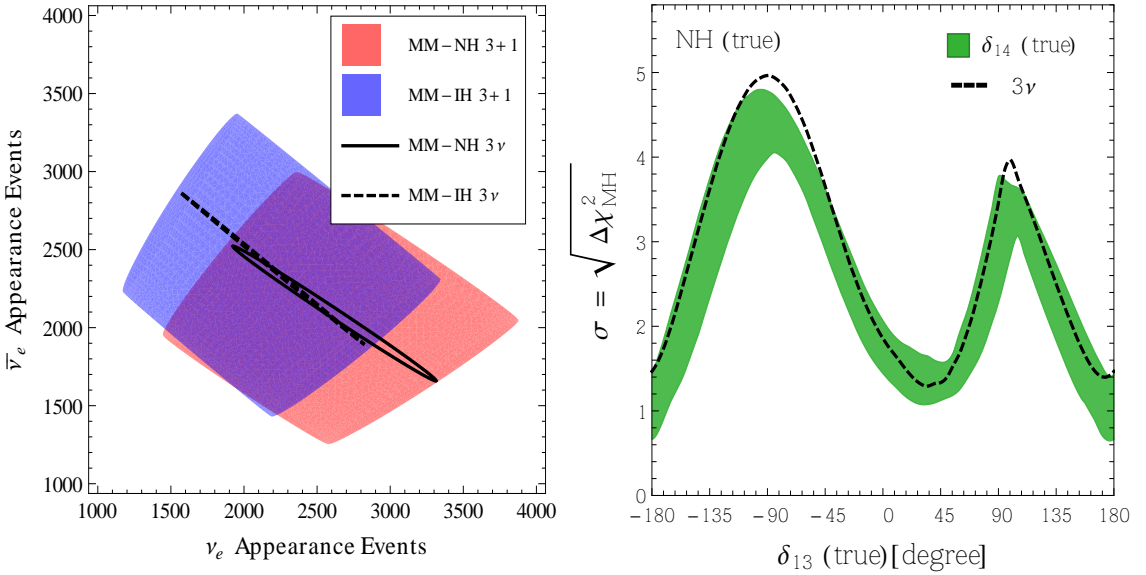


Figure 1. Left panel: bievents plot for 3-flavor (black ellipses) and 4-flavor case (colored blobs). Right panel: Discovery potential for identifying the correct hierarchy (NH) as a function of true δ_{13} . We have fixed true and test $\theta_{14} = \theta_{24} = 90^\circ$. The black dashed line represents the 3-flavor case, while the green band corresponds to the $3+1$ scheme. Such a band is obtained by varying the true value of δ_{14} in the range $[-\pi, \pi]$ and marginalizing the test value of δ_{14} in the same range.

4 Mass hierarchy discovery potential in the $3+1$ scheme

In this section, we treat the sensitivity of T2HK to the neutrino mass hierarchy. First of all we provide a discussion at the level of the electron neutrino events making use of the bievents plots. Then, we present the results of the full analysis.

The left panel of Fig. 1, represents the bi-event plots where the two axes report the number of ν_e (x -axis) and $\bar{\nu}_e$ (y -axis) events. The two ellipses correspond to the 3-flavor case and are obtained varying the CP phase δ_{13} in the range $[-\pi, \pi]$. The solid (dashed) ellipse refers to the NH (IH). The offset between the two ellipses is a direct consequence of matter effects, which act in opposite directions in the transition probability for the two cases of NH and IH. This offset confers to the experiments T2HK some sensitivity to the mass hierarchy. However, differently from DUNE (where matter effects are stronger), the separation of the two ellipses is not complete and one expects that the MH discovery potential is limited. In the $3+1$ scheme, there are two CP phases and their variation in the range $[-\pi, \pi]$ gives much more freedom. The scatter plots obtained varying the CP phases δ_{13} and δ_{14} are superimposed to the 3-flavor ellipses in the left panel Fig. 1. Despite the larger parameter freedom, we can observe that the separation of two blobs corresponding to NH and IH remains similar to that of the 3-flavor ellipses. Therefore, we expect that the discovery potential of the MH in the $3+1$ scheme will suffer only a mild deterioration with respect to the 3-flavor case.

refs. [43–46].

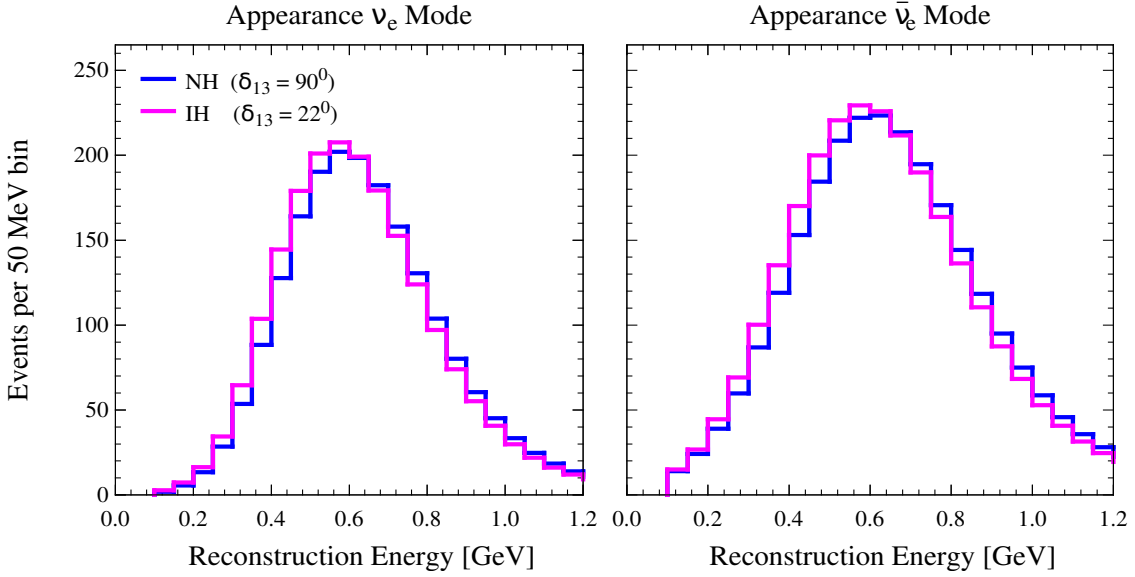


Figure 2. Energy spectra for neutrinos (left panel) and antineutrinos (right panel) for NH (blue lines) and IH (magenta lines). The values of the CP-phase for NH and IH have been chosen so that the total number of neutrino and antineutrino events are basically identical for the two hierarchies. In this case, the noticeable residual sensitivity to MH (4σ according to right panel of Fig. 1 for $\delta_{13} = 90^\circ$) is entirely provided by the energy shape information.

In the right panel of Fig. 1, we plot the MH discovery potential as a function of the true value of δ_{13} . We define the discovery potential as the statistical significance at which the wrong test hierarchy is rejected given a data set which is generated with the true hierarchy. Let us consider first the 3-flavor scenario. In this case the sensitivity to the MH (for NH as the true hierarchy choice) is represented by a black dashed line. Such a curve is obtained by marginalizing the test value of δ_{13} in the range $[-\pi, \pi]$ and θ_{23} (test) within the 3σ range allowed by the global analyses [26–28]. Although such a 3-flavor MH sensitivity curve has been already shown in several previous works [15, 36, 47–54], its behavior deserves some clarification. In fact, on the basis of the bievents plot on the left panel one would expect maximal sensitivity for $\delta_{13} = -90^\circ$, since the distance of the representative point on the (solid) NH ellipse (right lower point) has maximal distance from the IH ellipse. While this elementary feature is confirmed by the right panel Fig. 1, which presents a pronounced maximum ($\sim 5\sigma$) for $\delta_{13} \simeq -90^\circ$, the same figure also shows something unexpected. Quite surprisingly a good sensitivity ($\sim 4\sigma$) appears also for $\delta_{13} \simeq 90^\circ$. However, for such a value of δ_{13} , the bievents plot (see the ellipses in the left panel) shows that the distance of the representative point on the solid NH ellipse (left upper point) from the (dashed) IH ellipse is very close to zero. This is a well known fact (known as δ_{13} -MH degeneracy) which is supposed to reduce to zero the sensitivity to the MH. So the question arises where does the 4σ sensitivity found in the right panel Fig. 1 for $\delta_{13} = 90^\circ$ come from. The answer is that although the number of events cannot distinguish NH from IH for $\delta_{13} = 90^\circ$, the full energy

spectrum can. In Fig. 2 we elucidate this fact by showing, for the 3-flavor case, the neutrino (left panel) and antineutrino (right panel) spectra for the two choices (NH, $\delta_{13} = 90^\circ$) and (IH, $\delta_{13} = 22^\circ$), which correspond approximately to a common point in the 3-flavor bievents plot (i.e. equal number of neutrino and antineutrino events). Figure 2 clearly shows that the two spectra are different and therefore the spectral information provides sensitivity to the MH discrimination. Therefore, we conclude that the spectral information has a crucial role in the sensitivity to the MH and is able to break the δ_{13} -MH degeneracy for a wide range of the values of δ_{13} around 90° . Unfortunately, for values of δ_{13} around 45° and 180° , the spectral information is less effective and the sensitivity does not surpass the 2σ level. As far as we know, the role of the spectral information in the MH discrimination in T2HK has not been discussed before in the literature.

In the 3+1 scheme (green band in the right panel of Fig. 1), in addition to δ_{13} and θ_{23} , the marginalization is carried out over the CP phase δ_{14} . We have taken $\theta_{14} = \theta_{24} = 90^\circ$ both in data and fit. The spread of the band is due to the variation of the true value of δ_{14} in its entire range of $[-\pi, \pi]$. We observe that the qualitative behavior of the 3+1 band follows that of the 3-flavor case, and as expected, there is only a mild deterioration of the MH discovery potential. Also in this case the spectral information plays an important role in the MH discrimination. We can conclude that although the MH discovery potential of T2HK is quite limited⁵ it is rather robust with respect to the perturbations induced by a light sterile neutrino species.

5 CP-violation searches in the 3+1 scheme

In this section, we analyze the capability of T2HK of nailing down the enlarged CPV sector implied by the 3+1 scheme. Before showing the full numerical results we present a discussion at the level of bievents plots, which will serve as a valid guide to understand the results of the full simulations. As a first step we assess the sensitivity to the CPV induced by the CP phase δ_{13} in the 3-flavor framework. As a second step we show how the sensitivity to the CPV induced by δ_{13} changes in the 3+1 scheme. As a third step, we investigate the sensitivity to the non-standard CP phase δ_{14} (which appears only in the 3+1 scheme). Throughout the discussion, for the first time in the literature, we evidence the essential role of the energy spectrum in providing a minimal guaranteed sensitivity to the CPV induced by the new phase δ_{14} . Finally, we discuss the capability of reconstructing the true values of the two phases δ_{13} and δ_{14} .

5.1 CP-violation discovery potential

The sensitivity of CPV induced by a given (true) value of a CP phase $\delta_{ij}^{\text{true}}$ is defined as the statistical significance at which one can exclude the test hypothesis of no CPV, i.e. the (test) cases $\delta_{ij}^{\text{test}} = 0$ and $\delta_{ij}^{\text{test}} = \pi$. The qualitative behavior of the sensitivity to

⁵Although T2HK has a limited sensitivity to the mass hierarchy, Hyper-Kamiokande (HK) can settle this issue using the atmospheric neutrinos at more than 3σ C.L. for both NH and IH provided that $\sin^2 \theta_{23} > 0.45$ [55]. Combining beam and atmospheric neutrinos in HK, the mass hierarchy can be determined at more than 3σ (5σ) with five (ten) years of data [55].

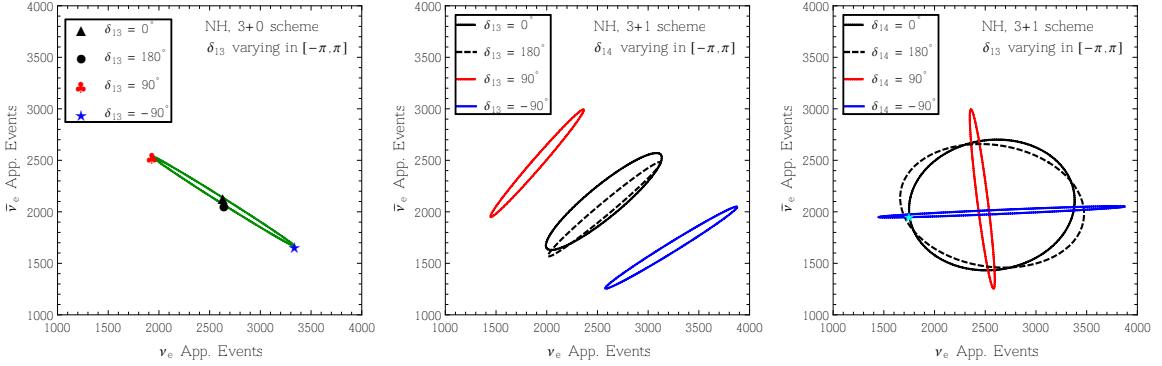


Figure 3. Bievents plots for the 3-flavor framework (left panel) and 3+1 scheme (central and right panels). In the left panel two black marks are located for the test cases of no CPV ($\delta_{13} = 0, \pi$) and two colored ones for the true cases corresponding to maximal CPV ($\delta_{13} = -\pi/2, \pi/2$). For completeness we draw also the (green) ellipse where the 3-flavor model lives, which is obtained by varying δ_{13} in the range $[-\pi, \pi]$. The non-zero distance between the black marks and the colored ones indicates that events counting can determine CPV induced by the phase δ_{13} in the 3ν case. In the 3+1 scheme a fixed value of δ_{13} is represented by an ellipse, where δ_{14} varies in the range $[-\pi, \pi]$. The non-zero minimal distance between the black ellipses and each of the two colored ones indicates that events counting is sensitive to CPV induced by the phase δ_{13} also in the 3+1 case. The right panel illustrates the sensitivity to the CPV induced by δ_{14} . In this case four ellipses are plotted for four fixed values of δ_{14} (while δ_{13} is varying in the range $[-\pi, \pi]$). Each of the two ellipses (blue and red) corresponding to maximal CPV induced by δ_{14} crosses the two ellipses (solid and dashed black) corresponding to no CPV induced by δ_{14} . In the (unlucky) crossing points the events counting is not sensitive to CPV induced by the new CP-phase δ_{14} . See the text for details.

the CPV induced by a given phase δ_{ij} can be traced by a careful inspection of opportune bievents plots. The three panels of Fig. 3 illustrate graphically the following three cases: i) CPV induced by δ_{13} in the 3-flavor framework (left panel); ii) CPV induced by δ_{13} in the 3+1 scheme (central panel); iii) CPV induced by δ_{14} in the 3+1 scheme (right panel). In all panels we have assumed NH for definiteness. In the standard 3-flavor scenario (left panel) there is only one (true) CP-phase ($\delta_{13}^{\text{true}}$), which is the running parameter over the green ellipse in the range $[-\pi, \pi]$. The two (inequivalent) CP conserving test points ($\delta_{13}^{\text{test}} = 0, \pi$) are indicated with a triangle and a circle. We also indicate two points of the ellipse corresponding to maximal CP violation ($\delta_{13}^{\text{true}} = -\pi/2, \pi/2$) with a star and a black club. According to the definition of the sensitivity given at the beginning of this subsection, the non-zero distance between any of the two (maximally) CP violating (true) points from both the CP conserving (test) points, guarantees that, in the 3-flavor scheme, events counting is sensitive to CPV induced by δ_{13} . The central panel of Fig. 3 concerns the 3+1 scheme and is meant to illustrate the sensitivity to CPV induced by δ_{13} in such an enlarged scheme. We recall that in the 3+1 scheme a given value of δ_{13} corresponds to an ellipse, whose running parameter is the other phase δ_{14} in its range $[-\pi, \pi]$ (for a detailed study of the properties of the 3+1 ellipses see [39]). The central panel reports four ellipses of which two (the black ones) correspond to the (inequivalent) CP conserving test cases ($\delta_{13}^{\text{test}} = 0, \pi$) and the other two (the colored ones) represent maximal CP violation

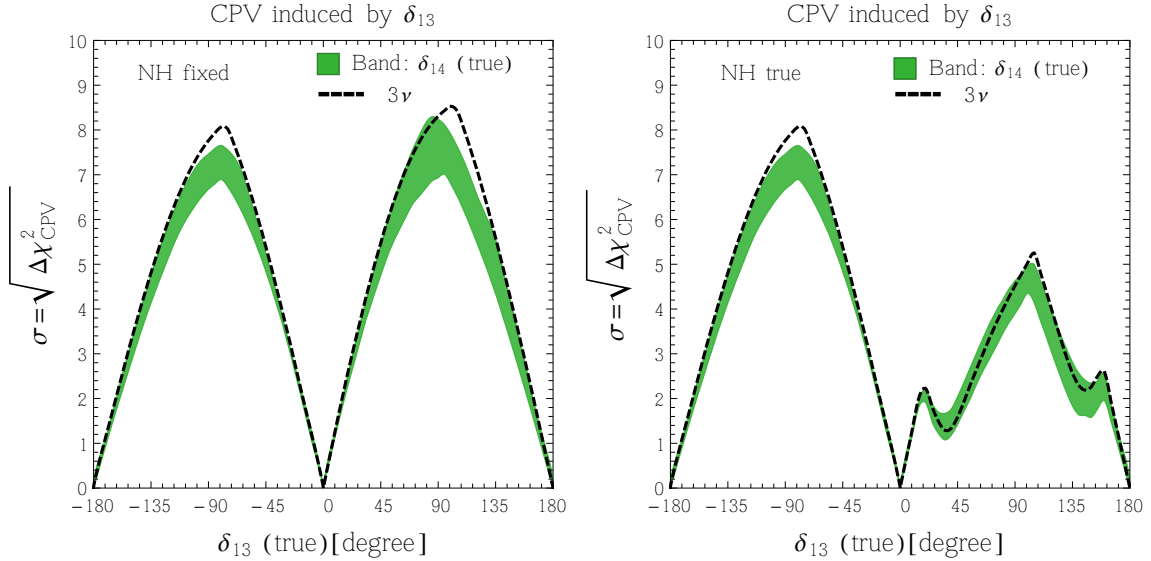


Figure 4. T2HK discovery potential of $\delta_{13} \neq (0, \pi)$. In the left panel the MH is fixed to be the NH (both true and test value). In the right panel the MH is marginalized with NH true. In both panels, the black dashed curve corresponds to the 3-flavor case. In 3+1 scenario, we fix the true and test values of $\theta_{14} = \theta_{24} = 90^\circ$. In both panels, the colored bands are obtained in the 3+1 scheme by varying the unknown value of the true δ_{14} in its entire range of $[-\pi, \pi]$ while marginalizing over test δ_{14} in the same range.

($\delta_{13}^{\text{true}} = -\pi/2, \pi/2$). In the 3+1 scheme, in order to decide if there is sensitivity to CPV (induced by δ_{13}) one has to look at the minimal distance between a generic point lying on one of the two colored ellipses (this point will correspond to a generic value of $\delta_{14}^{\text{true}}$) from the two black ellipses (where $\delta_{14}^{\text{test}}$ runs in the range $[-\pi, \pi]$). From the plot, we see that the major axes of the four ellipses are almost parallel, and as a consequence whatever is the point chosen on the colored ellipses (i.e., the value of $\delta_{14}^{\text{true}}$), its distance from the black ellipses is always non-zero. Also, we may observe that the minimal distance between colored and black ellipses is very similar (just slightly lower because the ellipses are not exactly parallel) to that found in the 3-flavor scheme between the CP violating cases (star, black club) and the CP conserving ones (triangle and circle). Therefore, we expect that in the 3+1 scheme, the sensitivity to CPV induced by δ_{13} will be only slightly lower than that achieved in the standard 3-flavor scenario. Finally, the right panel of Fig. 3 illustrates the sensitivity to the CPV induced by δ_{14} . In this case the four ellipses correspond to four fixed values of δ_{14} (while δ_{13} is varying in the range $[-\pi, \pi]$). Differently from the central panel, now the four ellipses have a completely different behavior. In particular, the two test CP conserving black ellipses ($\delta_{14}^{\text{test}} = 0, \pi$) are almost circular, while the two colored ellipses corresponding to maximal CP violation ($\delta_{14}^{\text{true}} = -\pi/2, \pi/2$) are almost degenerate with a line and are orthogonal to each other (this behavior was already found and discussed in [39]). As a result, the distance of a generic point located on one of the two colored ellipses (which will have a generic value of $\delta_{13}^{\text{true}}$) from the two black ellipses is not necessarily bigger than zero. In fact, each colored ellipse crosses a black ellipse in four points. Each of the

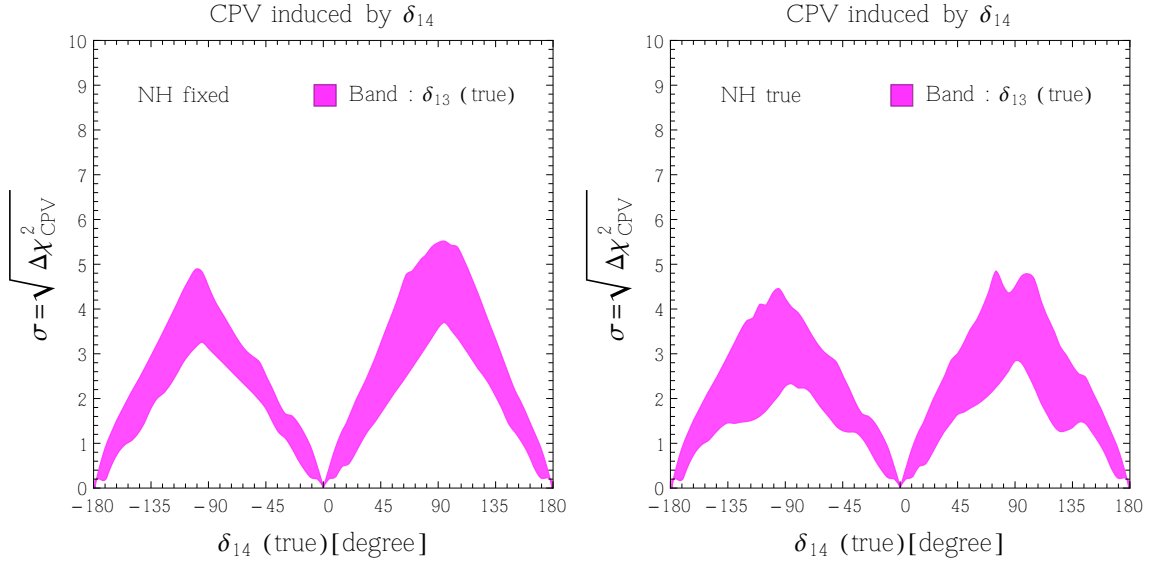


Figure 5. Discovery potential of $\delta_{14} \neq (0, \pi)$. In the left panel the MH is fixed to be the NH. In the right panel the MH is marginalized with NH as the true choice. In both cases we have taken true and test $\theta_{14} = \theta_{24} = 90^\circ$. The bands have been obtained by varying the true value of δ_{13} in its allowed range of $[-\pi, \pi]$ while marginalizing over its test value in the same range.

crossing points between a colored ellipse and a black one will correspond to a particular pair of values of the two phases $(\delta_{13}^{\text{true}}, \delta_{13}^{\text{test}})$. In such points the numbers of neutrino and antineutrino events are identical for maximal CPV and no CPV induced by δ_{14} and, as a consequence, events counting is completely insensitive to the CPV induced by δ_{14} . We have checked that such “unlucky pairs” approximately correspond to the sixteen possible combinations in couples of the four values $\delta_{13} = (-135^\circ, -45^\circ, 45^\circ, 135^\circ)$.⁶

In Fig. 4, we report the discovery potential of CPV induced by δ_{13} . In the left panel we have assumed that the hierarchy is known a priori and is NH. In the right panel we assume no a priori knowledge of the hierarchy generating the data with NH as the true choice and marginalizing over the two hierarchies. In this last case, the task of the experiment is more difficult because it has to identify both CPV and the MH. In both the panels, the black dashed curves correspond to the 3-flavor scenario and the green band to the 3+1 scheme. In the 3+1 scenario, we fix the true and test values of θ_{14} and θ_{24} to be 90° . In both the panels, the green bands are obtained by varying the unknown true value of δ_{14} in the range of $[-\pi, \pi]$ while marginalizing over its test value in the same range. In the left panel two maxima are present around $\delta_{13} \sim \pm 90^\circ$. In the right panel the height of the second maximum around $\delta_{13} \sim 90^\circ$ is drastically reduced as a result of the degeneracy between MH and the CP phase δ_{13} . Finally, we observe that the deterioration found in the 3+1 scheme is mild in agreement with the discussion made at the bievents level.

In Fig. 5, we display the discovery potential of CPV induced by δ_{14} . Like in the

⁶Note that in twelve of the sixteen combinations $\delta_{13}^{\text{true}}$ is much different from $\delta_{13}^{\text{test}}$. Hence a prior determination of δ_{13} with a good precision, imposing $\delta_{13}^{\text{test}} \simeq \delta_{13}^{\text{true}}$, would reduce the crossing points only two four.

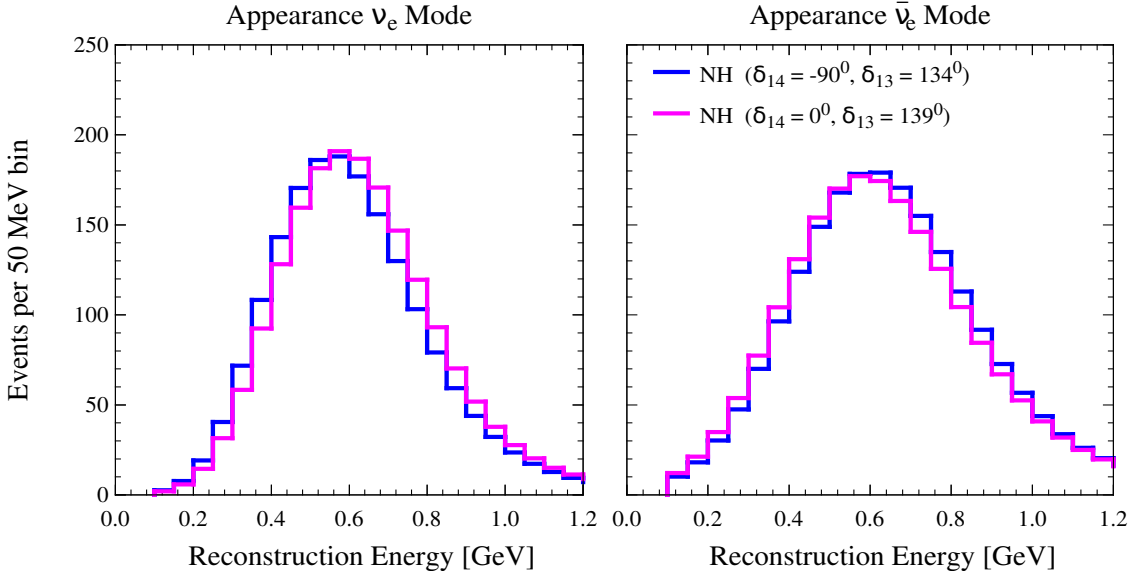


Figure 6. Energy spectra for neutrinos (left panel) and antineutrinos (right panel) obtained for NH. The magenta histograms correspond to a case of no CPV induced by δ_{14} ($\delta_{14} = 0$). The blue histograms correspond to a case of maximal CPV induced by δ_{14} ($\delta_{14} = -90^\circ$). The two values of δ_{13} have been chosen in order to have complete degeneracy at the level of both neutrino and antineutrino events. These choices of phases correspond to one of the sixteen crossing points in the right panel of Fig. 3 (therein indicated by a cyan star). The difference in the spectra is in this case the only source of sensitivity to the CPV induced by δ_{14} , which is $\sim 3.5\sigma$ according to the left panel of Fig. 5 for $\delta_{14} = -90^\circ$.

previous figure, in the left panel the hierarchy is fixed (NH) while in the right panel it is unknown (assuming the true hierarchy to be normal). In each panel, the bands have been obtained by varying the true values of the CP phase δ_{13} in the range $[-\pi, \pi]$ while marginalizing over their test values in the same range in the fit. Based on the discussion made at the bievents level one should expect that for unlucky values of $(\delta_{13}^{\text{true}}, \delta_{13}^{\text{test}})$ the sensitivity drops to zero. In contrast, the left panel of Fig. 5 shows that there is a guaranteed minimal sensitivity, which for the maximally CPV cases $\delta_{14}^{\text{true}} = \pm 90^\circ$ is roughly 3.5σ . This means that even in the unlucky cases of complete degeneracy at the level of the total (neutrino and antineutrino) events between the case of maximal CPV and that of no CPV, a residual sensitivity is provided by the energy spectral information. In Fig. 6 we elucidate this fact by showing the neutrino (left panel) and antineutrino (right panel) spectra for two cases that are degenerate at the events level. The first one corresponds to maximal CPV induced by $\delta_{14} = -90^\circ$ ($\delta_{13} = 134^\circ$) and the second one to no CPV induced by the same phase ($\delta_{14} = 0$, $\delta_{13} = 139^\circ$). This choice of the phases correspond to one of the sixteen crossing points in the bievents plot in the right panel of Fig. 3 (therein indicated by a cyan star). Figure 6 clearly shows that, although the number of (both neutrino and antineutrino) events is identical, the two spectra are different and therefore they provide

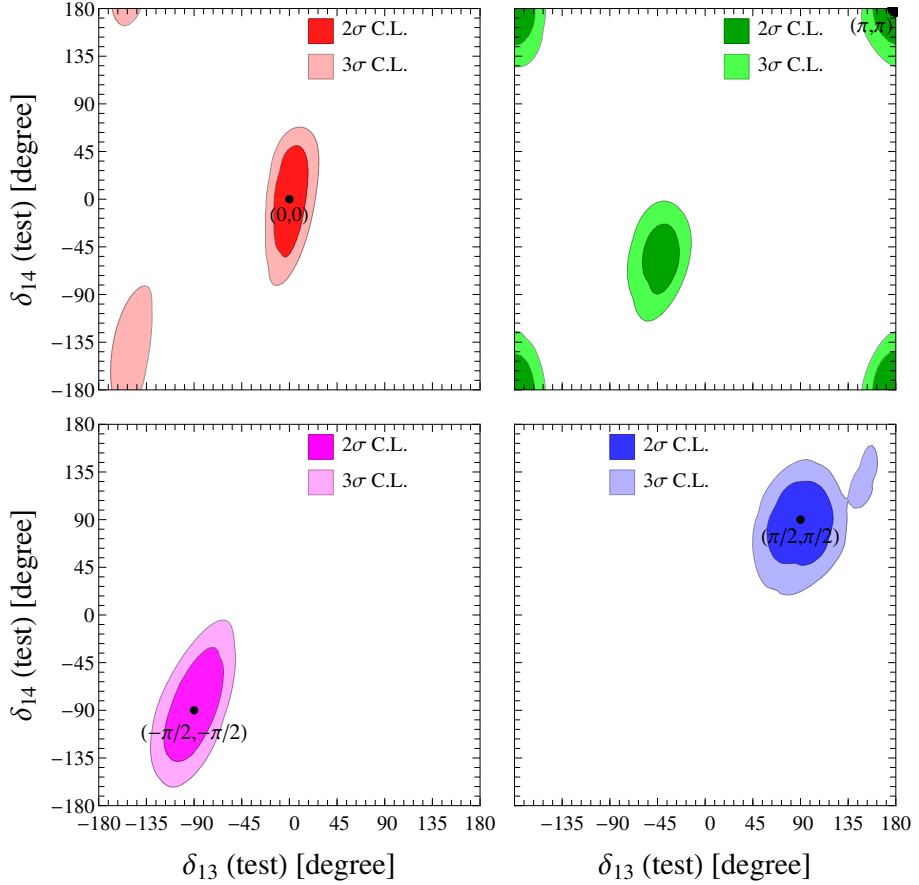


Figure 7. Reconstructed regions for the two CP phases δ_{13} and δ_{14} for the four benchmark pairs of their true values indicated in each panel. We have taken the NH as the true hierarchy and we have marginalized over the two possible hierarchies in the test model. The contours refer to 2σ and 3σ levels.

some sensitivity to the CPV induced by δ_{14} . As far as we know, the role of the spectral information in the CPV induced by the new CP phase δ_{14} has not been discussed before in the literature. Finally, we note that, there is a deterioration of the discovery potential to CPV induced by δ_{14} when going from the left panel (known hierarchy) to the right panel (unknown hierarchy) of Fig. 5. Also in this case, the spectral information guarantees a minimal degree of sensitivity, which for the maximally CPV cases $\delta_{14}^{\text{true}} = \pm 90^\circ$ is roughly 2.5σ .

5.2 Reconstruction of the CP phases

Until now, we have focused on the discovery potential of the CPV generated by the two CP phases δ_{13} and δ_{14} . Here, we investigate the capability of reconstructing the true values of the two CP phases. With this purpose we consider the four benchmark cases

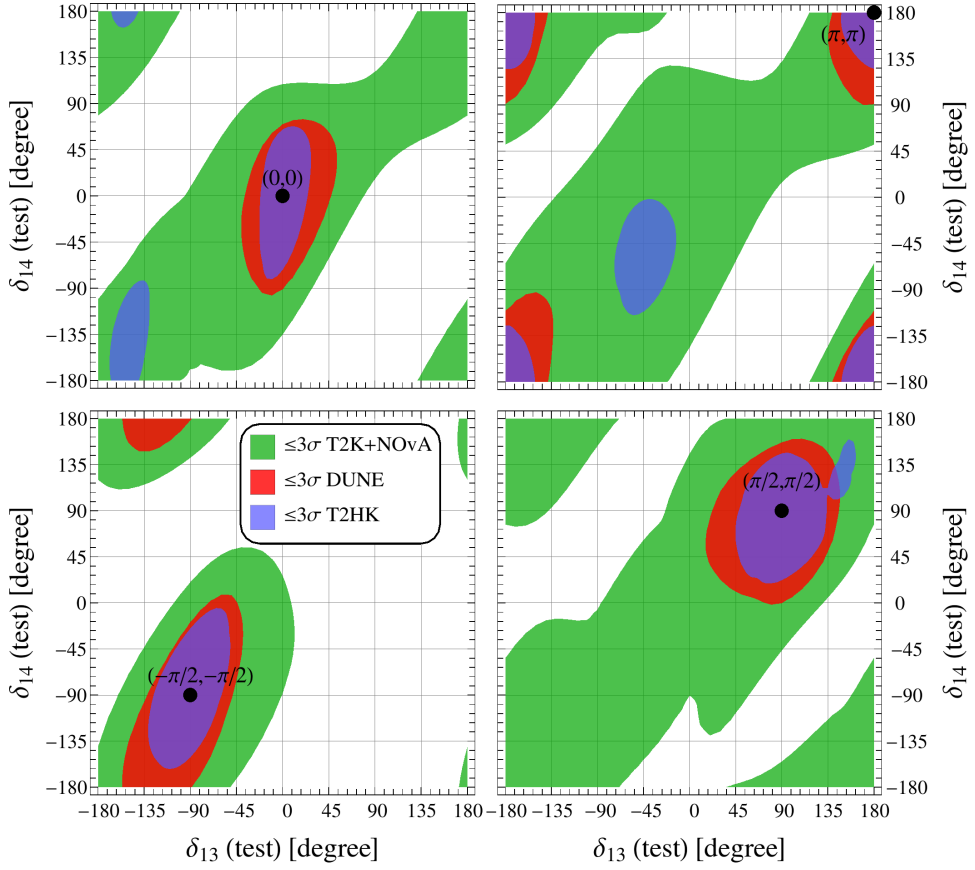


Figure 8. Reconstructed regions for the two CP phases δ_{13} and δ_{14} for three different experimental setups. We have taken the NH as the true hierarchy and we have marginalized over the two possible hierarchies in the test model. The contours correspond to the 3σ level.

displayed in Fig. 7. The two upper panels represent the CP-conserving scenarios $[0, 0]$ and $[\pi, \pi]$. The third and fourth panels represent two CP-violating cases $[-\pi/2, -\pi/2]$ and $[\pi/2, \pi/2]$. In each panel, we draw the regions reconstructed around the true values of δ_{13} and δ_{14} . In this plot we have taken the NH as the true hierarchy and we have marginalized over the two possible hierarchies in the test model. The two confidence levels correspond to 2σ and 3σ (1 d.o.f.). The typical 1σ level uncertainty on the reconstructed CP phases is approximately 15^0 (30^0) for δ_{13} (δ_{14}). We see however that spurious islands appear in three of the four cases considered. In first panel an island appears around $(\delta_{13}, \delta_{14}) = (-150^0, -150^0)$, in the second panel around⁷ $(\delta_{13}, \delta_{14}) = (-45^0, -45^0)$, in the fourth panel around $(\delta_{13}, \delta_{14}) = (150^0, 150^0)$. This misreconstruction is imputable to the

⁷We recall that both δ_{13} and δ_{14} are cyclic variables, therefore the four corners in the second panel of Fig. 7 form a unique region.

well known degeneracy between δ_{13} and $\text{sgn}(\Delta m_{31}^2)$. The combination of phases chosen for the third panel seems to be the most favorable one (no misreconstructed islands). This happens because in such a case the difference in the number of events for NH and IH is more pronounced and therefore there is a better discrimination of the MH (see the discussion in [39]). We have explicitly checked that if the MH is supposed to be known a priori (i.e. it is fixed and not marginalized in the fit), the spurious islands disappears in all cases. Therefore, our results show that in T2HK in order to have good reconstruction capabilities of the two CP phases, one needs the prior knowledge of the mass hierarchy.

We close this section by performing a comparison of the CP-phase reconstruction potential of three different experimental setups⁸ : T2K+NO ν A, DUNE and T2HK. In Fig. 8 we plot the reconstructed regions obtained by these three setups for the same benchmark values of the true phases chosen in Fig. 7. For visual clearness we report only the 3σ contours. The plots clearly show that there is huge gain when going from T2K+NO ν A to the new generation experiments DUNE and T2HK. Concerning these two last experiments, the figure shows that T2HK is slightly more precise than DUNE in reconstructing the region around the true values CP phases. However, while in T2HK there are small spurious islands, this does not happen in DUNE. This different behavior is rooted in the fact that the degeneracy between δ_{13} and $\text{sgn}(\Delta m_{31}^2)$ is less pronounced in DUNE. This, in turn, happens because DUNE can neatly separate the two hierarchies thanks to the larger matter effects.

6 Sensitivity to the octant of θ_{23}

The latest global fits of neutrino data indicate a preference for non-maximal θ_{23} with two nearly degenerate solutions, one in the lower octant ($\theta_{23} < \pi/4$), and the other in the higher octant ($\theta_{23} > \pi/4$). The resolution of this octant ambiguity is a crucial target of next-generation LBL experiments. In a recent work [57] it was shown that in the 3+1 scheme the sensitivity of the future LBL experiment DUNE to the the θ_{23} octant can be deteriorated in a drastic way. Here we perform a similar analysis to check if the same conclusion holds for T2HK. Figure 9 displays the discovery potential for identifying the true octant in the plane $[\delta_{13}, \sin^2 \theta_{23}]$ (true) assuming NH as true choice. The left (right) panel represents the results obtained in 3ν (3+1) scheme. In the 3+1 case we marginalized over the CP phase δ_{14} (true) (in addition to all the test parameters) since such a phase is unknown. Hence, the outcome of this procedure provides the minimal guaranteed sensitivity. The three contours correspond, respectively, to 2σ , 3σ and 4σ confidence levels (1 d.o.f.). The comparison of the two panels neatly shows that in the 3+1 scheme no minimal sensitivity is guaranteed in the entire plane. We have checked that similar results are valid also in the case of IH as true MH. Hence, we confirm that also in T2HK, like in DUNE, the identification of the octant of θ_{23} is problematic when one works in the enlarged 3+1 framework.

⁸For a detailed discussion of the CP-phases reconstruction potential of T2K+NO ν A and DUNE, see respectively [39] and [56].

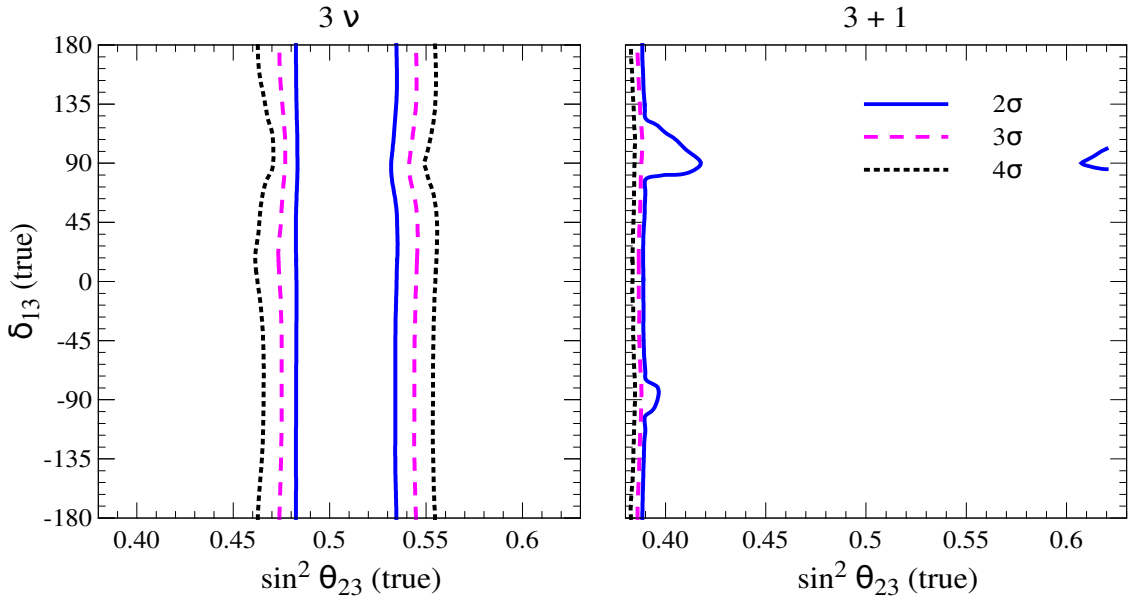


Figure 9. Discovery potential for identifying the correct octant assuming NH as true choice. The left (right) panel corresponds to the 3ν ($3+1$) case. In the 3ν case, we marginalize away $(\theta_{23}, \delta_{13})$ (test). In the $3+1$ case, in addition, we marginalize away also δ_{14} (true) and δ_{14} (test) fixing $\theta_{14} = \theta_{24} = 90^\circ$.

7 Conclusions and Outlook

We have investigated the capability of T2HK to provide information on the mass hierarchy, the CP phases, and the octant of θ_{23} , in the presence of one light sterile neutrino species. Working in $3+1$ scheme, we have found that the discovery potential of the mass hierarchy is rather robust with respect to the perturbations induced by the sterile species. We have also found that the discovery potential of CPV induced by the standard CP phase δ_{13} gets only slightly deteriorated compared to the standard 3ν case. In particular, the maximal sensitivity (reached around $\delta_{13} \sim \pm 90^\circ$) decreases from 8σ to 7σ if the amplitude of the two new mixing angles θ_{14} and θ_{24} is close to that of θ_{13} . The sensitivity to the CPV due to δ_{14} can reach 5σ but is below 3σ for most of the true values of such a phase. We have also investigated the reconstruction capability of the two phases δ_{13} and δ_{14} . The typical 1σ uncertainty on δ_{13} (δ_{14}) is $\sim 15^\circ$ (30°). Finally, we have assessed the sensitivity to the octant of θ_{23} . We have found that in T2HK there can be a complete loss of sensitivity for unlucky values of the two CP phases δ_{13} and δ_{14} . We highlighted, for the first time in the literature, the crucial role of the spectral energy shape information in improving the sensitivity both to the mass hierarchy and to CPV induced by the new CP-phase δ_{14} . Notably, we have shown that events counting, for unlucky values of the CP-phase δ_{13} , may be completely insensitive to CPV induced by the new CP-phase δ_{14} , and that an appreciable sensitivity can be guaranteed only by the energy spectral information. We

hope that our present study to look for a light sterile neutrino in T2HK will be a useful addition to the list of important physics topics which can be addressed using the proposed T2HK setup.

Acknowledgments

S.K.A. and S.S.C. are supported by the DST/INSPIRE Research Grant [IFA-PH-12], Department of Science & Technology, India. A part of S.K.A.’s work was carried out at the International Centre for Theoretical Physics (ICTP), Trieste, Italy. It is a pleasure for him to thank the ICTP for the hospitality and support during his visit via SIMONS Associateship. S.K.A would like to thank T. Kobayashi for useful discussions. A.P. is supported by the grant “Future In Research” *Beyond three neutrino families*, Fondo di Sviluppo e Coesione 2007-2013, APQ Ricerca Regione Puglia, Italy, “Programma regionale a sostegno della specializzazione intelligente e della sostenibilità sociale ed ambientale”. A.P. acknowledges partial support by the research project *TAsP* funded by the Instituto Nazionale di Fisica Nucleare (INFN).

References

- [1] K. N. Abazajian et al., *Light Sterile Neutrinos: A White Paper*, [arXiv:1204.5379](https://arxiv.org/abs/1204.5379).
- [2] A. Palazzo, *Phenomenology of light sterile neutrinos: a brief review*, *Mod. Phys. Lett. A* **28** (2013) 1330004, [[arXiv:1302.1102](https://arxiv.org/abs/1302.1102)].
- [3] S. Gariazzo, C. Giunti, M. Laveder, Y. F. Li, and E. M. Zavanin, *Light sterile neutrinos*, [arXiv:1507.08204](https://arxiv.org/abs/1507.08204).
- [4] T. Lasserre, *Light Sterile Neutrinos in Particle Physics: Experimental Status*, *Phys. Dark Univ.* **4** (2014) 81–85, [[arXiv:1404.7352](https://arxiv.org/abs/1404.7352)].
- [5] N. Klop and A. Palazzo, *Imprints of CP violation induced by sterile neutrinos in T2K data*, *Phys. Rev. D* **91** (2015), no. 7 073017, [[arXiv:1412.7524](https://arxiv.org/abs/1412.7524)].
- [6] S. Pascoli and T. Schwetz, *Prospects for neutrino oscillation physics*, *Adv.High Energy Phys.* **2013** (2013) 503401.
- [7] S. K. Agarwalla, S. Prakash, and S. Uma Sankar, *Exploring the three flavor effects with future superbeams using liquid argon detectors*, *JHEP* **1403** (2014) 087, [[arXiv:1304.3251](https://arxiv.org/abs/1304.3251)].
- [8] S. K. Agarwalla, *Physics Potential of Long-Baseline Experiments*, *Adv.High Energy Phys.* **2014** (2014) 457803, [[arXiv:1401.4705](https://arxiv.org/abs/1401.4705)].
- [9] G. Feldman, J. Hartnell, and T. Kobayashi, *Long-baseline neutrino oscillation experiments*, *Adv.High Energy Phys.* **2013** (2013) 475749, [[arXiv:1210.1778](https://arxiv.org/abs/1210.1778)].
- [10] L. Stanco, *Next Generation of Neutrino Studies and Facilities*, [arXiv:1511.09409](https://arxiv.org/abs/1511.09409).
- [11] D. Hollander and I. Mocioiu, *Minimal 3+2 sterile neutrino model at LBNE*, *Phys. Rev. D* **91** (2015), no. 1 013002, [[arXiv:1408.1749](https://arxiv.org/abs/1408.1749)].
- [12] J. M. Berryman, A. de Gouv  a, K. J. Kelly, and A. Kobach, *Sterile neutrino at the Deep Underground Neutrino Experiment*, *Phys. Rev. D* **92** (2015), no. 7 073012, [[arXiv:1507.03986](https://arxiv.org/abs/1507.03986)].

- [13] R. Gandhi, B. Kayser, M. Masud, and S. Prakash, *The impact of sterile neutrinos on CP measurements at long baselines*, *JHEP* **11** (2015) 039, [[arXiv:1508.06275](https://arxiv.org/abs/1508.06275)].
- [14] P. Coloma, D. V. Forero, and S. J. Parke, *DUNE sensitivities to the mixing between sterile and tau neutrinos*, [arXiv:1707.05348](https://arxiv.org/abs/1707.05348).
- [15] S. Choubey, D. Dutta, and D. Pramanik, *Imprints of a light Sterile Neutrino at DUNE, T2HK and T2HKK*, [arXiv:1704.07269](https://arxiv.org/abs/1704.07269).
- [16] S. Choubey, D. Dutta, and D. Pramanik, *Measuring the Sterile Neutrino CP Phase at DUNE and T2HK*, [arXiv:1711.07464](https://arxiv.org/abs/1711.07464).
- [17] A. Donini and D. Meloni, *The 2+2 and 3+1 four family neutrino mixing at the neutrino factory*, *Eur. Phys. J.* **C22** (2001) 179–186, [[hep-ph/0105089](https://arxiv.org/abs/hep-ph/0105089)].
- [18] A. Donini, M. Lusignoli, and D. Meloni, *Telling three neutrinos from four neutrinos at the neutrino factory*, *Nucl. Phys.* **B624** (2002) 405–422, [[hep-ph/0107231](https://arxiv.org/abs/hep-ph/0107231)].
- [19] A. Donini, M. Maltoni, D. Meloni, P. Migliozzi, and F. Terranova, *3+1 sterile neutrinos at the CNGS*, *JHEP* **12** (2007) 013, [[arXiv:0704.0388](https://arxiv.org/abs/0704.0388)].
- [20] A. Dighe and S. Ray, *Signatures of heavy sterile neutrinos at long baseline experiments*, *Phys. Rev.* **D76** (2007) 113001, [[arXiv:0709.0383](https://arxiv.org/abs/0709.0383)].
- [21] A. Donini, K.-i. Fuki, J. Lopez-Pavon, D. Meloni, and O. Yasuda, *The Discovery channel at the Neutrino Factory: numu to nutau pointing to sterile neutrinos*, *JHEP* **08** (2009) 041, [[arXiv:0812.3703](https://arxiv.org/abs/0812.3703)].
- [22] O. Yasuda, *Sensitivity to sterile neutrino mixings and the discovery channel at a neutrino factory*, in *Physics beyond the standard models of particles, cosmology and astrophysics. Proceedings, 5th International Conference, Beyond 2010, Cape Town, South Africa, February 1-6, 2010*, pp. 300–313, 2011. [arXiv:1004.2388](https://arxiv.org/abs/1004.2388).
- [23] D. Meloni, J. Tang, and W. Winter, *Sterile neutrinos beyond LSND at the Neutrino Factory*, *Phys. Rev.* **D82** (2010) 093008, [[arXiv:1007.2419](https://arxiv.org/abs/1007.2419)].
- [24] B. Bhattacharya, A. M. Thalapillil, and C. E. M. Wagner, *Implications of sterile neutrinos for medium/long-baseline neutrino experiments and the determination of θ_{13}* , *Phys. Rev.* **D85** (2012) 073004, [[arXiv:1111.4225](https://arxiv.org/abs/1111.4225)].
- [25] A. Donini, P. Hernandez, J. Lopez-Pavon, M. Maltoni, and T. Schwetz, *The minimal 3+2 neutrino model versus oscillation anomalies*, *JHEP* **07** (2012) 161, [[arXiv:1205.5230](https://arxiv.org/abs/1205.5230)].
- [26] P. F. de Salas, D. V. Forero, C. A. Ternes, M. Tortola, and J. W. F. Valle, *Status of neutrino oscillations 2017*, [arXiv:1708.01186](https://arxiv.org/abs/1708.01186).
- [27] F. Capozzi, E. Di Valentino, E. Lisi, A. Marrone, A. Melchiorri, and A. Palazzo, *Global constraints on absolute neutrino masses and their ordering*, *Phys. Rev.* **D95** (2017), no. 9 096014, [[arXiv:1703.04471](https://arxiv.org/abs/1703.04471)].
- [28] I. Esteban, M. C. Gonzalez-Garcia, M. Maltoni, I. Martinez-Soler, and T. Schwetz, *Updated fit to three neutrino mixing: exploring the accelerator-reactor complementarity*, *JHEP* **01** (2017) 087, [[arXiv:1611.01514](https://arxiv.org/abs/1611.01514)].
- [29] F. Capozzi, C. Giunti, M. Laveder, and A. Palazzo, *Joint short- and long-baseline constraints on light sterile neutrinos*, *Phys. Rev.* **D95** (2017), no. 3 033006, [[arXiv:1612.07764](https://arxiv.org/abs/1612.07764)].
- [30] S. Gariazzo, C. Giunti, M. Laveder, and Y. F. Li, *Updated Global 3+1 Analysis of Short-BaseLine Neutrino Oscillations*, *JHEP* **06** (2017) 135, [[arXiv:1703.00860](https://arxiv.org/abs/1703.00860)].

[31] M. Dentler, . Hernndez-Cabezudo, J. Kopp, M. Maltoni, and T. Schwetz, *Sterile Neutrinos or Flux Uncertainties? - Status of the Reactor Anti-Neutrino Anomaly*, *JHEP* **11** (2017) 099, [[arXiv:1709.04294](https://arxiv.org/abs/1709.04294)].

[32] K. Abe, T. Abe, H. Aihara, Y. Fukuda, Y. Hayato, et al., *Letter of Intent: The Hyper-Kamiokande Experiment — Detector Design and Physics Potential —*, [[arXiv:1109.3262](https://arxiv.org/abs/1109.3262)].

[33] **Hyper-Kamiokande Working Group** Collaboration, K. Abe et al., *A Long Baseline Neutrino Oscillation Experiment Using J-PARC Neutrino Beam and Hyper-Kamiokande*, [[arXiv:1412.4673](https://arxiv.org/abs/1412.4673)].

[34] **Hyper-Kamiokande Proto-Collaboration** Collaboration, K. Abe et al., *Physics potential of a long-baseline neutrino oscillation experiment using a J-PARC neutrino beam and Hyper-Kamiokande*, *PTEP* **2015** (2015) 053C02, [[arXiv:1502.05199](https://arxiv.org/abs/1502.05199)].

[35] A. Para and M. Szleper, *Neutrino oscillations experiments using off-axis NuMI beam*, [[hep-ex/0110032](https://arxiv.org/abs/hep-ex/0110032)].

[36] **Hyper-Kamiokande proto-** Collaboration, K. Abe et al., *Physics Potentials with the Second Hyper-Kamiokande Detector in Korea*, [[arXiv:1611.06118](https://arxiv.org/abs/1611.06118)].

[37] P. Huber, M. Lindner, and W. Winter, *Simulation of long-baseline neutrino oscillation experiments with GLoBES (General Long Baseline Experiment Simulator)*, *Comput.Phys.Commun.* **167** (2005) 195, [[hep-ph/0407333](https://arxiv.org/abs/hep-ph/0407333)].

[38] P. Huber, J. Kopp, M. Lindner, M. Rolinec, and W. Winter, *New features in the simulation of neutrino oscillation experiments with GLoBES 3.0: General Long Baseline Experiment Simulator*, *Comput.Phys.Commun.* **177** (2007) 432–438, [[hep-ph/0701187](https://arxiv.org/abs/hep-ph/0701187)].

[39] S. K. Agarwalla, S. S. Chatterjee, A. Dasgupta, and A. Palazzo, *Discovery Potential of T2K and NOvA in the Presence of a Light Sterile Neutrino*, *JHEP* **02** (2016) 111, [[arXiv:1601.05995](https://arxiv.org/abs/1601.05995)].

[40] A. M. Dziewonski and D. L. Anderson, *Preliminary reference earth model*, *Physics of the Earth and Planetary Interiors* **25** (1981) 297–356.

[41] P. Huber, M. Lindner, and W. Winter, *Superbeams versus neutrino factories*, *Nucl. Phys.* **B645** (2002) 3–48, [[hep-ph/0204352](https://arxiv.org/abs/hep-ph/0204352)].

[42] G. L. Fogli, E. Lisi, A. Marrone, D. Montanino, and A. Palazzo, *Getting the most from the statistical analysis of solar neutrino oscillations*, *Phys. Rev.* **D66** (2002) 053010, [[hep-ph/0206162](https://arxiv.org/abs/hep-ph/0206162)].

[43] E. Ciuffoli, J. Evslin, and X. Zhang, *Confidence in a neutrino mass hierarchy determination*, *JHEP* **01** (2014) 095, [[arXiv:1305.5150](https://arxiv.org/abs/1305.5150)].

[44] M. Blennow, P. Coloma, P. Huber, and T. Schwetz, *Quantifying the sensitivity of oscillation experiments to the neutrino mass ordering*, *JHEP* **1403** (2014) 028, [[arXiv:1311.1822](https://arxiv.org/abs/1311.1822)].

[45] M. Blennow, *On the Bayesian approach to neutrino mass ordering*, *JHEP* **01** (2014) 139, [[arXiv:1311.3183](https://arxiv.org/abs/1311.3183)].

[46] J. Elevant and T. Schwetz, *On the determination of the leptonic CP phase*, *JHEP* **09** (2015) 016, [[arXiv:1506.07685](https://arxiv.org/abs/1506.07685)].

[47] J. Liao, D. Marfatia, and K. Whisnant, *Nonstandard neutrino interactions at DUNE, T2HK and T2HKK*, *JHEP* **01** (2017) 071, [[arXiv:1612.01443](https://arxiv.org/abs/1612.01443)].

- [48] S. Fukasawa, M. Ghosh, and O. Yasuda, *Complementarity Between Hyperkamiokande and DUNE in Determining Neutrino Oscillation Parameters*, *Nucl. Phys.* **B918** (2017) 337–357, [[arXiv:1607.03758](https://arxiv.org/abs/1607.03758)].
- [49] P. Ballett, S. F. King, S. Pascoli, N. W. Prouse, and T. Wang, *Sensitivities and synergies of DUNE and T2HK*, [arXiv:1612.07275](https://arxiv.org/abs/1612.07275).
- [50] M. Ghosh and O. Yasuda, *Effect of systematics in the T2HK, T2HKK, and DUNE experiments*, *Phys. Rev.* **D96** (2017), no. 1 013001, [[arXiv:1702.06482](https://arxiv.org/abs/1702.06482)].
- [51] S. K. Raut, *T2HK and T2HKK: Does more matter matter?*, [arXiv:1703.07136](https://arxiv.org/abs/1703.07136).
- [52] S. K. Agarwalla, M. Ghosh, and S. K. Raut, *A hybrid setup for fundamental unknowns in neutrino oscillations using T2HK (ν) and μ -DAR ($\bar{\nu}$)*, *JHEP* **05** (2017) 115, [[arXiv:1704.06116](https://arxiv.org/abs/1704.06116)].
- [53] K. Chakraborty, K. N. Deepthi, and S. Goswami, *Spotlighting the sensitivities of T2HK, T2HKK and DUNE*, [arXiv:1711.11107](https://arxiv.org/abs/1711.11107).
- [54] S. C, K. N. Deepthi, and R. Mohanta, *A comprehensive study of the discovery potential of NOvA, T2K and T2HK experiments*, *Adv. High Energy Phys.* **2016** (2016) 9139402, [[arXiv:1408.6071](https://arxiv.org/abs/1408.6071)].
- [55] **Hyper-Kamiokande Proto** Collaboration, M. Yokoyama, *The Hyper-Kamiokande Experiment*, in *Proceedings, Prospects in Neutrino Physics (NuPhys2016): London, UK, December 12-14, 2016*, 2017. [arXiv:1705.00306](https://arxiv.org/abs/1705.00306).
- [56] S. K. Agarwalla, S. S. Chatterjee, and A. Palazzo, *Physics Reach of DUNE with a Light Sterile Neutrino*, *JHEP* **09** (2016) 016, [[arXiv:1603.03759](https://arxiv.org/abs/1603.03759)].
- [57] S. K. Agarwalla, S. S. Chatterjee, and A. Palazzo, *Octant of θ_{23} in danger with a light sterile neutrino*, *Phys. Rev. Lett.* **118** (2017), no. 3 031804, [[arXiv:1605.04299](https://arxiv.org/abs/1605.04299)].